

Diverse Image Inpainting with Bidirectional and Autoregressive Transformers

Yingchen Yu^{1*} Fangneng Zhan^{1*} Rongliang Wu¹ Jianxiong Pan² Kaiwen Cui¹
 Shijian Lu^{1†} Feiyong Ma² Xuansong Xie² Chunyan Miao¹

¹ Nanyang Technological University ² DAMO Academy, Alibaba Group

{yingchen001, ronglian001, kaiwen001}@e.ntu.edu.sg, {fnzhan, shijian.lu, ascymiao}@ntu.edu.sg
 {jianxiong.pjx, feiyong.mfy}@alibaba-inc.com, xingtong.xxs@taobao.com

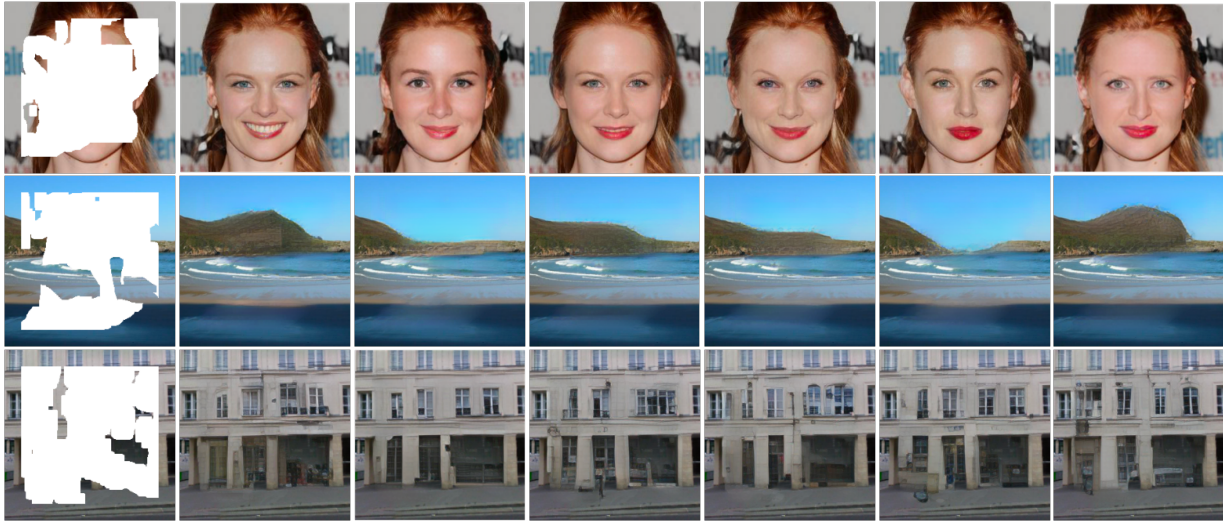


Figure 1. The proposed BAT-Fill inherits the merits of transformers and CNNs and allows to generate high-resolution contents without being constrained by the quadratic complexity of self-attention in transformers. With a novel bidirectional autoregressive transformer (BAT), BAT-Fill captures deep bidirectional contexts for autoregressive generation of diverse contents in image inpainting. Evaluations over multiple public datasets show that the proposed method can generate realistic and reasonable image contents (the three diverse completion samples from top to bottom are from datasets CelebA-HQ [20], Places2 [62], and Paris StreetView [32], respectively).

Abstract

Image inpainting is an underdetermined inverse problem, it naturally allows diverse contents that fill up the missing or corrupted regions reasonably and realistically. Prevalent approaches using convolutional neural networks (CNNs) can synthesize visually pleasant contents, but CNNs suffer from limited perception fields for capturing global features. With image-level attention, transformers enable to model long-range dependencies and generate diverse contents with autoregressive modeling of pixel-sequence distributions. However, the unidirectional attention in transformers is suboptimal as corrupted regions can have arbitrary shapes with contexts from arbitrary directions. We propose BAT-Fill, an image inpainting framework with a

novel bidirectional autoregressive transformer (BAT) that models deep bidirectional contexts for autoregressive generation of diverse inpainting contents. BAT-Fill inherits the merits of transformers and CNNs in a two-stage manner, which allows to generate high-resolution contents without being constrained by the quadratic complexity of attention in transformers. Specifically, it first generates pluralistic image structures of low resolution by adapting transformers and then synthesizes realistic texture details of high resolutions with a CNN-based up-sampling network. Extensive experiments over multiple datasets show that BAT-Fill achieves superior diversity and fidelity in image inpainting qualitatively and quantitatively.

*Equal contribution

†Corresponding author

1. Introduction

Image inpainting aims to synthesize visually plausible yet semantically reasonable contents in corrupted images. It has a wide range of applications in various image editing tasks such as object removal [3], photo restoration [40], image manipulation [49], etc. As an ill-posed problem, image inpainting naturally allows numerous solutions as long as the restored images are realistic and semantically reasonable as illustrated in Fig. 1. However, it remains a great challenge to synthesize diverse while realistic contents that maintain integrity and consistency with the uncorrupted image regions, especially when the corrupted image regions are large and rich in complex textures and structures.

Recently, CNN-based inpainting [32, 49, 30, 26] has achieved remarkable progress by training with reconstruction and adversarial losses over large-scale datasets. CNNs can learn rich and robust texture representations leveraging the local inductive bias and spatial invariance of convolution operations, but they suffer from two major constraints in image inpainting. First, they do not capture global information well due to the limited receptive fields and the local nature of convolution operations. Though stacking convolution and pooling mitigates this issue to some extent, the issue remains due to the spatial translation equivariance in convolutions. Several methods employ a Coarse-to-Fine strategy [49, 30, 23] to address this issue by first inferring structural information and then refining appearance details, but they still struggle in generating reasonable structures when missing regions are large. Second, most CNN-based methods learn one-to-one mapping and can only produce deterministic inpainting. A few recent studies [61, 59] attempt for diverse inpainting with variational auto-encoder (VAE) networks [22] but the inpainting quality is often compromised while generating complex structural and texture patterns due to the limited capacity of parametric distributions [60].

Leveraging the powerful attention mechanisms, transformers [39] can naturally establish long-range dependencies and model global information well. In addition, generative models using transformers typically estimate data distributions by using an autoregressive model [8] that naturally supports diverse generations. However, transformers have two constraints while handling image inpainting tasks. First, the computational cost of transformers increases quadratically, which severely hinders the application of transformers in high-resolution image generation and inpainting. Second, autoregressive models are optimized to encode unidirectional context only, hence the ensuing contexts after the current position will not be attended. As a result, when modeling the distribution of missing pixels in a raster-scan order, the informative contexts of valid future pixels are substantially ignored in autoregression. Nevertheless, image inpainting requires bidirectional

context information (before and after the current position) for optimal generation of missing or corrupted image regions with arbitrary shapes and sizes. Though masked language models (MLM) like BERT [11] exploit bidirectional contexts for data reconstruction, they ignore the output dependency and predict all masked tokens separately, which oversimplify the modeling of the context dependency in natural language or images [46].

In this paper, we propose BAT-Fill, a novel two-stage framework that inherits the merits of transformers and CNNs for diverse and high-fidelity image inpainting. The first stage focuses on structure reconstruction, which adapts transformers to model the global structural information and recover the diverse yet coherent image structures effectively. Specially, we designed a bidirectional and autoregressive transformer (BAT) that marries the best of autoregressive modeling and MLM to model deep bidirectional contexts in an autoregressive manner. In the proposed BAT, we permute the input sequence by sorting the valid and missing pixels and start autoregressive modeling at the position of the first missing pixel. With all available contexts in front, BAT can exploit bidirectional contexts and spatial dependency simultaneously. The second stage focuses on the generation of fine-grained texture, which exploits a CNN-based texture generator to learn local texture representations. It synthesizes realistic textures for the missing region under the guidance of the restored structures as well as the style of valid/visible pixels in the corrupted image.

The main contributions of this work can be summarized in three aspects. First, we propose a diverse inpainting framework BAT-Fill that employs transformers and CNNs for the recovery of diverse image structures and generation of realistic texture details, respectively. Second, we design a novel bidirectional and autoregressive transformer (BAT) that captures bidirectional information and establishes output dependency simultaneously. Third, extensive experiments over multiple datasets show that the proposed method achieves superior performance as compared with the state-of-the-art in both inpainting quality and inpainting diversity.

2. Related Work

2.1. Image Inpainting

As an ill-posed problem, realistic and high-fidelity image inpainting is a challenging task that has been studied for years. Based on the inpainting outcome, most existing image inpainting methods can be broadly classified into two categories including deterministic image inpainting and diverse image inpainting.

2.1.1 Deterministic Image Inpainting

Traditional methods address image inpainting challenge through either image diffusion [5, 1] or using image patches [3, 14, 9]. However, diffusion-based methods often introduce diffusion-related blurs, which tends to fail while the missing or corrupted image regions are large [6, 2, 4]. Patch-based methods can work well for the inpainting of stationary background with repeating patterns. However, they struggle in completing large missing regions of complex scenes as the patch-based approach relies heavily on patch-wise matching of low-level features.

Generative adversarial networks (GANs) [13] have been investigated extensively in various image synthesise tasks such as image translation [31, 35, 18, 52, 50, 54], image editing [47, 43, 42], image composition [24, 57, 56, 51, 55, 53], etc. Specifically for image inpainting, Pathak *et al.* [32] first apply adversarial learning to the image inpainting task. To further improve the adversarial learning within local regions, Iizuka *et al.* [17] introduce an extra local discriminator to enforce the local consistency. As the local discriminator uses fully-connected layers and can only deal with missing regions of fixed shapes, Yu *et al.* [48] inherit the discriminator from PatchGAN [18] due to its great success in image translation. Yan *et al.* [45] propose patch-swap to make use of distant feature patches for the better inpainting quality. Liu *et al.* [25] design partial convolutions to alleviate the negative influence of the masked regions. Yu *et al.* [49] present a novel free-form image inpainting system based on an end-to-end generative network with gated convolutions. To generate reasonable structures and realistic textures, Nazeri *et al.* [30] and Xu *et al.* [44] utilize edge maps as structural guidance for image inpainting, and Ren *et al.* [34] instead propose to use edge-preserved smooth images as structural guidance. Liu *et al.* [27] propose feature equalizations to improve the consistency between structures and textures. As aforementioned methods focus on reconstructing the ground truth instead of generating pluralistic inpainting, they are constraint to generate a deterministic inpainting image for each incomplete image.

2.1.2 Diverse Image Inpainting

To achieve pluralistic image inpainting with plausible filling contents, Zheng *et al.* [61] propose a VAE-based network with a dual pipeline, which trades off between reconstructing ground truth and maintaining the diversity of the inpainting results. Similarly, Zhao *et al.* [59] project both the masked input and reference image into a common space by optimizing the KL-divergence between encoded features and $\mathcal{N}(\mathbf{0}, \mathbf{I})$ distribution to achieve diversified sampling and inpainting.

Although the above methods achieve certain diversities to some extent, their completion quality is limited due to

variational training. We instead propose to model discrete distribution of the structural information with a transformer architecture which naturally enables diverse image completion, more details to be discussed in the ensuing subsections.

2.2. Transformers in Vision

Transformer has emerged as a powerful tool to model the interactions between sequences regardless of the relative position. Specially, Vaswani *et al.* [39] employ transformers for image classification by treating an image as a sequence of patches. DETR [7] utilizes transformer decoder to model object detection as an end-to-end dictionary lookup problem with learnable queries, thus removing the hand-crafted processes such as Non-Maximal Suppression (NMS). Based on DETR, deformable DETR [63] further introduces a deformable attention layer to focus on a sparse set of contextual elements which achieves fast convergence and better detection performance. Recently, Vision Transformer (ViT) [12] showed that pure-transformer networks can also achieve excellent image classification performance as compared with CNN-based methods. DeiT [38] further extends ViT by introducing a novel distillation approach. BoTNet [37] replaces the spatial 3×3 convolution layers with multi-head self-attention in certain stages of the original ResNet [15], demonstrating very competitive performance on different visual recognition tasks.

Different from previous methods, we propose a novel Bidirectional and Autoregressive Transformer (BAT) which inherits the advantages of autoregressive models and bidirectional models and achieves superior image inpainting performance.

3. Proposed Method

As illustrated in Fig. 2, the proposed BAT-Fill consists of two major parts including a diverse-structure generator for the reconstruction of coarse image structures and a texture generator for the generation of fine-grained texture details. The diverse-structure generator incorporates and adapts a transformer architecture that models the distribution of global structural information and recovers complete and coherent low-resolution structures S_1, S_2, \dots, S_N given a *Masked Image* I_m as input. Under the guidance of coarse structure $S_i, i \in [1, N]$ and corrupted image I_m , the *Texture Generator* synthesizes high-resolution fine-grained texture to produce the *Inpainting Results* I_{out} . Once the full model is trained, we can sample different image structures $S_i, i \in [1, N]$ by the diverse-structure generator and thus generate diverse inpainting results with the texture generator, more details to be discussed in the ensuing subsections.

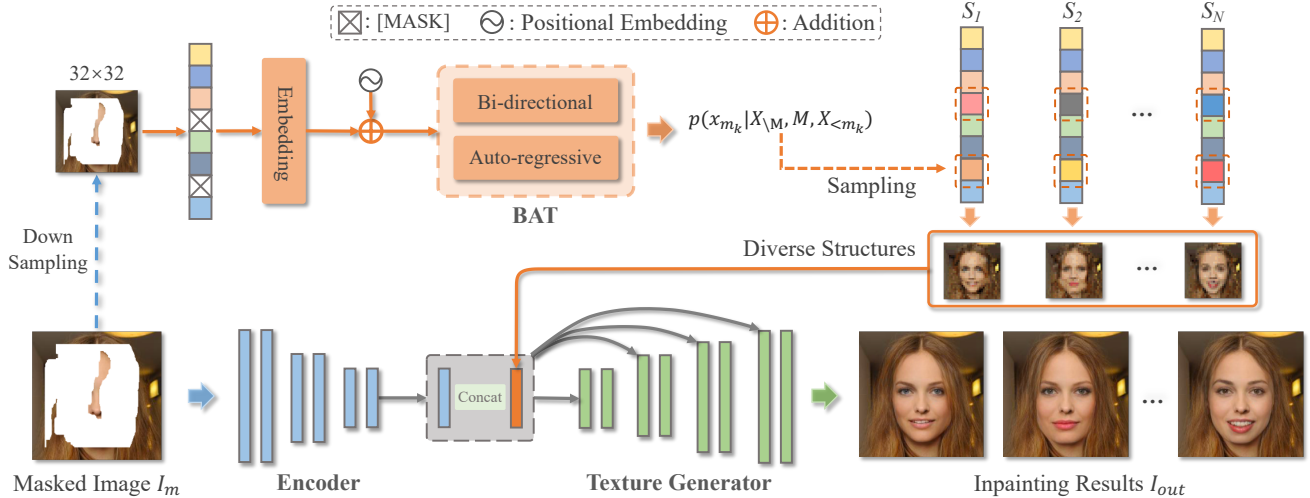


Figure 2. Overview of the proposed image inpainting method: Given a *Masked Image I_m* , the proposed *BAT-Fill* first *Down Sample* it to a lower resolution and feed the down-sampled image to the *Bidirectional Autoregressive Transformer (BAT)* for the recovery of *Diverse Structures*. Taking the recovered image structures and image style features (extracted by the *Encoder*) as inputs, the *Texture Generator* synthesizes high-resolution texture and produce the *Inpainting Results I_{out}* .

3.1. Diverse-structure Generator

3.1.1 Context Representation

Due to the quadratic complexity incurred by self-attention, transformer struggles in handling high-resolution images. Take an RGB image of context length $L = 256 \times 256 \times 3$ as an example. It involves tens of billions of attention logits that are hard to fit into a GPU. To alleviate the memory cost, we propose to represent the structure information in a low-resolution image with the size of $32 \times 32 \times 3$ since global image structures can be well reconstructed with low-resolution images. In addition, the transformer requires discrete variables and RGB images have 8-bit color representation (with $2^8=256$ intensity levels) in each channel. Hence generative model needs to predict one color from 256^3 colors for each image pixel. To further reduce the dimensionality while faithfully representing images, we follow Chen *et al.* [8] and extract a color palette of size 512×3 from the ImageNet [10] dataset. The color palette is generated by k -means clustering of RGB pixel values with $k=512$, and each pixel in the low-resolution structure image is encoded to its discrete representation by searching the index of the nearest element in the color palette. With the discrete representation, we flatten the 2D low-resolution image into a 1-D sequence and replace the elements in the missing regions with a special token [MASK] following BERT [11].

3.1.2 Bidirectional and Autoregressive Transformer

Autoregressive (AR) modeling and masked language modeling (MLM) in BERT [11] are two representative objectives for exploiting large language corpora in lan-

guage processing tasks. Given a discrete sequence $X = \{x_1, x_2, \dots, x_L\}$ where L is the length of X , AR model is optimized by maximizing the unidirectional likelihood:

$$\log P(x; \theta) = \mathbb{E}_X \sum_{t=1}^L \log P(x_t | X_{< t}; \theta), \quad (1)$$

where θ is the parameters of the model. In contrast, MLM aims to reconstruct corrupted data with the masked positions $M = \{m_1, m_2, \dots, m_K\}$, where K is the number of masked tokens. Each masked position of the corrupted data is indicated by [MASK]. Denoting the masked tokens as X_M and unmasked tokens as $X_{\setminus M}$, the objective of MLM can be formulated by:

$$\log P(X_M | X_{\setminus M}; \theta) = \mathbb{E}_X \sum_{m_k \in M} \log P(x_{m_k} | X_{\setminus M}; \theta). \quad (2)$$

AR and MLM differ from two aspects as defined in Eqs. 1 and 2. The first aspect lies with *output dependency*, where MLM predicts the masked tokens separately and independently which may oversimplify the complex context dependency in the data [36]. As a comparison, AR factorizes the predicted tokens with the product rule, which establishes the output dependency and produces better predictions. The second aspect lies with *context dependency*, where AR is only conditioned on the tokens up to the current position (in a fixed order), while MLM has access to bidirectional contextual information. Therefore, MLM is more suitable for image inpainting as the missing or corrupted image regions often have arbitrary shapes with rich variation in the neighboring background.

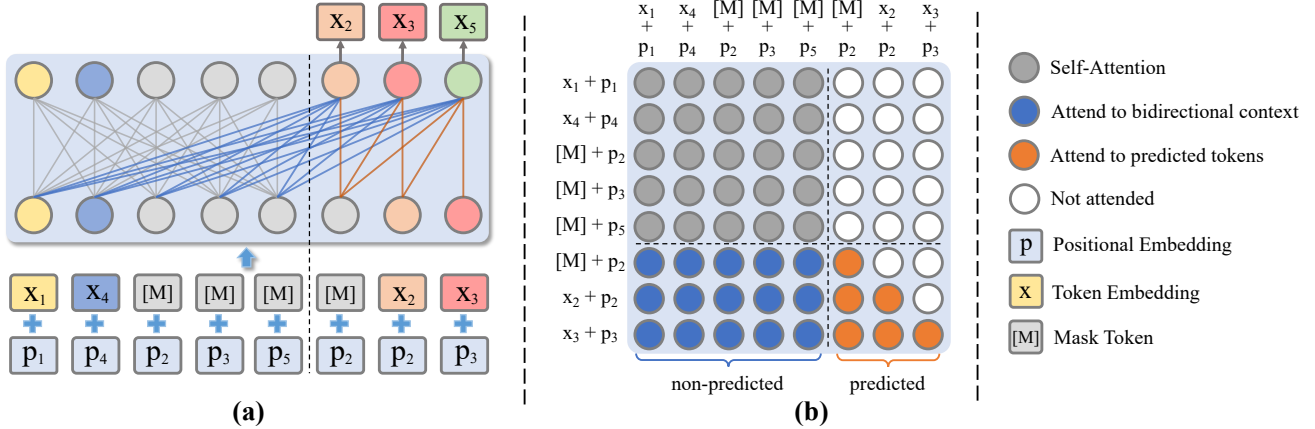


Figure 3. Illustrations of *BAT* and its attention mask. (a) All unmasked tokens (*i.e.* X_1, X_4) is permuted to the front of the sequence which is followed by masked tokens with positional embedding (*i.e.* p_2, p_3, p_5). It provides bidirectional context for the autoregressive modeling of masked tokens (*i.e.* X_2, X_3, X_5). (b) *BAT* allows to attend non-predicted tokens and previously predicted tokens for the prediction of masked future tokens. For example, while predicting X_3 , the model could attend to X_1, X_4 (non-predicted tokens) and X_2 (previously predicted token) simultaneously. Meanwhile, the future tokens are not attended to prevent information leakage in autoregressive modeling.

We propose a novel Bidirectional and Autoregressive Transformer (*BAT*) that inherits the advantages of AR and MLM to achieve bidirectional context modeling and output dependency simultaneously. The training objective of the *BAT* is formulated by:

$$\mathcal{L}_{BAT} = \mathbb{E}_X \sum_{m_k \in M} \log P(x_{m_k} | X_{\setminus M}, M, X_{< m_k}; \theta). \quad (3)$$

We first project all the tokens into a d -dimensional token embedding and add a learnable position embedding over the token embedding to preserve the positional information. Unlike XLNet [46] which randomly permutes the input sequence to capture the bidirectional context, we permute all unmasked tokens $X_{\setminus \Pi}$ in the front while maintaining the original order of the masked tokens for better predicting their positions. Moreover, the positional information of all masked tokens will be conditioned for better modeling of the full input sequence (e.g. the counts and positions of masked tokens in the sequence). The proposed *BAT* model is then adopted to predict the masked tokens as illustrated in Fig. 3.

As shown in Fig. 3, there is a masked sequence $X = \{x_1, [M], [M], x_4, [M]\}$ ($[M]$ is the short of [MASK]) with length $L = 5$ and positions 2, 3, 5 being masked. After permutation and inserting the full mask tokens, we have the non-predicted tokens $(X_{\setminus M}, M) = (x_1, x_4, [M], [M], [M])$ which provides the bidirectional context. For the predicted part, we have the input tokens $([M], x_2, x_3)$ to predict their corresponding next tokens *i.e.* (x_2, x_3, x_5) . Here we use the mask token instead of x_1 to predict x_2 to encourage the leverage of positional information. We apply bidirectional modeling [11] to non-predicted tokens and autoregressive modeling to the predicted tokens

to avoid future information leakage. For example, while predicting x_3 , the model could attend to x_4 in non-predicted tokens and meanwhile the previously ‘predicted’ token x_2 . Hence, we could capture bidirectional context and establish output dependency simultaneously with the proposed *BAT*.

3.1.3 Transformer Architecture

In this work, we adapt GPT [33] as our network architecture. The network is a decoder-only transformer that consists of \mathcal{N} stacked decoder blocks. Given an intermediate embedding H^n at the n -th layer, the decoder block can be formulated by:

$$H^n = H^n + \text{MA}(\text{LN}(H^n)) \quad (4)$$

$$H^{n+1} = H^n + \text{MLP}(\text{LN}(H^n)), \quad (5)$$

where *MA*, *LN* and *MLP* stand for multihead self-attention, layer normalization, and fully-connected layers, respectively. For self-attention, we apply a customized mask to the $L \times L$ matrix of attention logits as illustrated in Fig. 3. At the final layer of the transformer, a learnable linear projection is employed to map $H^{\mathcal{N}}$ to logits, which parameterizes the conditional distribution for each pixel.

During inference, we follow the raster-scan order to predict each masked token bidirectionally and autoregressively. We adopt a top- \mathcal{K} sampling strategy to randomly sample from the \mathcal{K} most likely next words. The predicted token is then concatenated with the input sequence as conditions for the generation of next masked token. This process repeats iteratively until all the masked tokens are sampled. Finally, the generated discrete sequence can be converted back to the RGB values with the aforementioned color palette.

3.2. Texture Generator

3.2.1 Network Architecture

As the inpainting diversity can be achieved by sampling the reconstructed structures S , we take the advantages of efficiency and texture representation capacity of CNNs to learn a deterministic mapping between low-resolution structures S and high-resolution completed image I_{out} . The texture generator thus utilizes CNN layers and adversarial training to up-sample the reconstructed structures and replenish high-fidelity texture details by leveraging the styles of the valid pixels of input image I_m . In particular, we employ two encoders to encode the low-resolution structures and input images into two high-level CNN representations of the same dimension. We then concatenate them together as the input of a few consecutive residual blocks with different dilation rates. Finally, a SPADE [31] generator is employed to incorporate the modulated style of input images and gradually up-sample the texture features to the target resolution. Meanwhile, all vanilla convolutions are replaced by gated convolution [49].

3.2.2 Loss Functions

The training of the texture generator is driven by the combination of several losses including a reconstruction loss, an adversarial loss, and a perceptual loss. For clarity, we denote the texture generator as G_t , the ground truth as I_{gt} , and the completed image as I_{out} . Firstly, a reconstruction loss \mathcal{L}_{rec} between I_{out} and I_{gt} can be measured as follows:

$$\mathcal{L}_{rec} = \|I_{out} - I_{gt}\|_1,$$

Besides, a CNN-based discriminator D together with an adversarial loss is employed to synthesize fine texture details. Specifically, the texture generator G_t and discriminator D are jointly trained with hinge loss [18], where the adversarial losses for the discriminator and generator are defined by:

$$\begin{aligned}\mathcal{L}_{adv}^D &= \mathbb{E}_{I_{gt}}[ReLU(1 - D(I_{gt}))] + \mathbb{E}_{I_{out}}[ReLU(1 + D(I_{out}))] \\ \mathcal{L}_{adv}^{G_t} &= -\mathbb{E}_{I_{out}}[D(I_{out})],\end{aligned}$$

Next, we penalize the perceptual and semantic discrepancy via the perceptual loss [19] with a pretrained VGG-19 network:

$$\begin{aligned}\mathcal{L}_{perc} &= \sum_i \lambda_i \|\Phi_i(I_{out}) - \Phi_i(I_{gt})\|_1 \\ &\quad + \lambda_l \|\Phi_l(I_{out}) - \Phi_l(I_{gt})\|_2,\end{aligned}$$

where λ_i are balancing weights, Φ_i is the activation of i -th layer of the VGG-19 model (including *relu1_2*, *relu2_2*,

relu3_2, *relu4_2* and *relu5_2*), Φ_l represents the activation maps of *relu4_2* layer which mainly extracts semantic feature. The texture generator is trained by optimizing the combination of aforementioned losses:

$$\mathcal{L}_{G_t} = \min_{G_t} \max_D (\lambda_{rec} \mathcal{L}_{rec} + \lambda_{adv} \mathcal{L}_{adv}^{G_t} + \lambda_{perc} \mathcal{L}_{perc}),$$

where λ_{rec} , λ_{adv} , and λ_{perc} are empirically set at 1.0, 1.0 and 0.2, respectively, in our implementation.

4. Experiments

4.1. Experimental Settings

4.1.1 Datasets

We conduct experiments over three public datasets that have different characteristics as listed:

- CelebA-HQ [20]: It is a high-quality version of the human face dataset CelebA [28] with 30,000 aligned face images. We follow the split in [49] that produces 28,000 training images and 2,000 validation images, where 1,000 validation images are randomly sampled in evaluations.
- Places2 [62]: It consists of more than 1.8M natural images of 365 different scenes. We randomly sampled 1,000 images from the validation set in evaluations.
- Paris StreetView [32]: It is a collection of street view images in Paris, which contains 14,900 training images and 100 validation images.

4.1.2 Compared Methods

We compare our method with a number of state-of-the-art methods as listed:

- GC [49]: It is also known as DeepFill v2, a two-stage method that leverages gated convolutions.
- EC [30]: It is a two-stage method that first predicts salient edges to guide the generation.
- MEDFE [26]: It is a mutual encoder-decoder that treats features from deep and shallow layers as structures and textures of an input image.
- PIC [61]: It is a probabilistically principled framework that leverages VAE to generate diverse image inpainting.

4.1.3 Evaluation Metrics

We perform evaluations by using five widely adopted evaluation metrics: 1) Fréchet Inception Score (FID) [16] that evaluates the perceptual quality by measuring the distribution distance between the synthesized images and real images; 2) mean ℓ_1 error; 3) peak signal-to-noise ratio (PSNR); 4) structural similarity index (SSIM) [41] with a window size of 51; 5) Learned Perceptual Image Patch Similarity (LPIPS) [58] that evaluates the diversity of generated

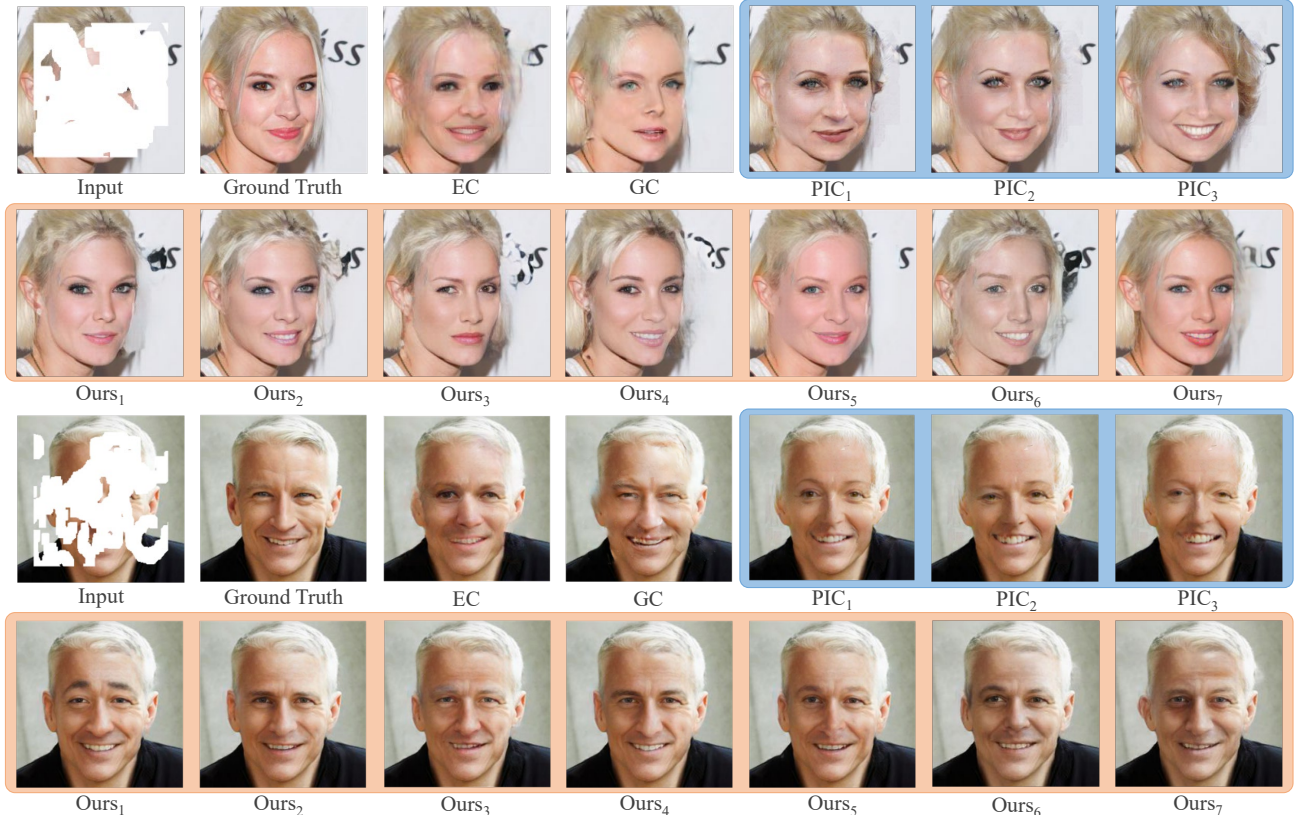


Figure 4. Qualitative comparisons of the proposed BAT-Fill with the state-of-the-art: BAT-Fill generates more realistic and diverse image inpainting over the dataset CelebA-HQ[20] with irregular masks.

images. The average scores of LPIPS are calculated between random pairs of sampled inpainting results.

4.1.4 Implementation Details

The proposed method is implemented in PyTorch. The network is trained using 256×256 images with random irregular masks [25]. The diverse-structure generator and texture generator are trained using 256×256 images with random irregular masks [25]. We train the diverse-structure generator with AdamW [29] with $\beta_1 = 0.9$, $\beta_2 = 0.95$ and learning rate of $3e-4$ following [8]. For the texture generator, we use Adam optimizer [21] with $\beta_1 = 0$ and $\beta_2 = 0.9$, and set the learning rate at $1e-4$ and $4e-4$ for the generator and discriminators, respectively. Learning rate decay is applied for the training of both networks, and the experiments are conducted on 4 NVIDIA(R) Tesla(R) V100 GPU.

4.2. Quantitative Evaluation

Extensive quantitative evaluations have been conducted over the three datasets with irregular masks [25]. The irregular masks in the experiments are categorized according to the mask ratios, and an additional category ‘random’ is evaluated which randomly samples masks with ratios vary-

ing from 20% to 60%. The performance of the compared methods was acquired by using the publicly available pre-trained models or implementation codes.^{1 2 3 4}.

We compare the proposed method with both deterministic and diverse image inpainting methods. Note that all reference metrics such as ℓ_1 , SSIM, and PSNR are in favor of deterministic inpainting methods where the prediction is directly compared with the ground truth. We would also highlight the comparison with the diverse inpainting method PIC [61]. Following the setting of PIC, we randomly sample 50 inpainting images per masked image and use them to evaluate the inpainting diversity. Among the 50 inpainting, the top 10 as sorted by the classification scores of the discriminator, and one random sample from the top 10 is used to evaluate the image quality. Different from PIC, our method adapts the top-50 sampling strategy and use all random samples for fair comparisons, which means our

¹https://github.com/JiahuiYu/generative_inpainting

²<https://github.com/knazeri/edge-connect>

³<https://github.com/KumapowerLIU/Rethinking-Inpainting-MEDFE>

⁴<https://github.com/lyndonzheng/Pluralistic-Inpainting>



Figure 5. Qualitative comparison the proposed BAT-Fill with the state-of-the-art: BAT-Fill generates more realistic and diverse image inpainting over datasets Places2 [62] (upper example) and Paris StreetView [32] (bottom example) with irregular masks.

method directly generates the stochastic inpainting without the additional filtering.

Table 2 shows the inpainting performance over the dataset Paris StreetView [32]. Compared with deterministic methods GC, EC, and MEDFE, the proposed method achieves the best FID scores over different mask ratios and consistently outperforms the diverse inpainting method PIC in both inpainting quality (FID) and inpainting diversity (LPIPS). In addition, Table 1 shows the inpainting performance over CelebA-HQ [20] and Places2 [62]. For CelebA-HQ, our method consistently outperforms all compared methods, especially in FID scores. For Places2, our method achieves comparable performance with deterministic methods in all evaluation metrics, and it generally outperforms them in FID scores. In addition, the numerical results of BAT-Fill suggest a clear superiority over the diverse inpainting method PIC [61].

4.3. Qualitative Evaluations

Figs. 4 and 5 show the qualitative comparisons between BAT-Fill and the state-of-the-art image inpainting methods over the validation set of CelebA-HQ [20], Places2 [62] and Paris StreetView [32].

We first evaluate and compare BAT-Fill with EC [30],

GC [49], and PIC [61] on CelebA-HQ [20] which contains facial images with similar semantics. As shown in Fig. 4, though EC [30] and GC [49] can synthesize complete facial images with reasonable semantics, they tend to generate distorted facial structures and artifacts in the missing regions which degrades inpainting greatly. In addition, EC [30] and GC [49] can only generate deterministic inpainting, which limits their applicability clearly. Both PIC [61] and BAT-Fill can generate diverse inpainting. However, the PIC generated images share similar makeups and facial features and thus have limited diversity. As a comparison, the BAT-Fill generated facial images vary across a wide range of makeups and facial features and contain much less artifacts, demonstrating that BAT-Fill can produce more diverse and realistic inpainting.

Next, we evaluate and compare BAT-Fill with EC [30], GC [49], MEDFE [26], and PIC [61] on the datasets Places2 [62] and Paris StreetView [32] where images have various semantics. As shown in Fig. 5, EC [30], GC [49] and MEDFE [26] tend to generate blurs and even corrupted texture in the inpainting images. The PIC synthesized images suffer from unreasonable semantics and limited diversity as shown in the first row and the third row, respectively. As a comparison, BAT-Fill is able to generate plausible images

Table 1. Quantitative comparison of the proposed BAT-Fill with state-of-the-art methods over CelebA-HQ [20] and Places2 [62] validation images (1,000) with irregular masks [25] (* denotes that we trained the model based on official implementations). For each metric, the best score is highlighted in **bold**, and the best score for diverse inpainting methods (*i.e.* PIC [61] and Ours) is highlighted in underline.

Methods	Dataset	FID↓			ℓ_1 (%) ↓			PSNR↑			SSIM↑		
		20-40%	40-60%	Random	20-40%	40-60%	Random	20-40%	40-60%	Random	20-40%	40-60%	Random
EC* [30]	CelebA-HQ [20]	9.06	16.45	12.46	2.19	4.71	3.40	26.60	22.14	24.45	0.923	0.823	0.877
GC [49]		14.12	22.80	18.10	2.70	5.19	3.88	25.17	21.21	23.32	0.907	0.805	0.858
PIC [61]		10.21	18.92	14.12	2.50	5.65	4.00	25.92	20.82	23.46	0.919	0.780	0.852
Ours		6.32	12.50	9.33	1.91	4.57	3.18	27.82	22.40	25.21	0.944	0.834	0.890
EC [30]	Places2 [62]	32.31	54.05	42.81	3.21	6.32	4.78	23.56	19.81	21.63	0.866	0.704	0.784
GC [49]		43.24	64.28	53.99	4.39	7.99	6.24	21.28	17.83	19.53	0.800	0.630	0.713
MEDFE [26]		38.35	74.28	55.26	3.27	7.26	5.28	23.68	18.77	21.17	0.871	0.679	0.773
PIC [61]		43.38	74.04	58.19	4.18	8.46	6.37	22.17	18.02	20.04	0.821	0.600	0.708
Ours		27.15	57.15	41.69	3.10	7.38	5.28	24.01	18.95	21.39	0.879	0.672	0.774

Table 2. Quantitative comparison of the proposed BAT-Fill with state-of-the-art methods over Paris StreetView [32] validation images (100) with irregular masks [25] (* denotes that we trained the model based on official implementations). For each metric, the best score is highlighted in **bold**, and the best score for diverse inpainting methods (*i.e.* PIC [61] and Ours) is highlighted in underline.

Metrics	Mask Ratio	Methods				
		EC [30]	GC* [49]	MEDFE [26]	PIC [61]	Ours
FID↓	20-40%	42.81	71.02	36.84	56.83	36.19
ℓ_1 (%) ↓		2.63	3.56	2.29	3.43	<u>2.70</u>
PSNR↑		26.76	23.95	27.64	24.80	<u>26.52</u>
SSIM↑		0.874	0.796	0.898	0.817	<u>0.864</u>
LPIPS↑		N/A	N/A	N/A	0.046	0.076
FID↓	40-60%	72.78	98.32	77.26	90.91	64.20
ℓ_1 (%) ↓		5.18	6.31	5.54	7.47	<u>5.83</u>
PSNR↑		22.77	20.83	22.01	20.12	<u>21.89</u>
SSIM↑		0.712	0.631	0.704	0.570	<u>0.678</u>
LPIPS↑		N/A	N/A	N/A	0.127	0.147
FID↓	Random	55.29	84.16	54.99	72.16	48.19
ℓ_1 (%) ↓		3.63	4.64	3.58	4.94	<u>3.96</u>
PSNR↑		25.04	22.61	25.24	22.97	<u>24.50</u>
SSIM↑		0.806	0.727	0.818	0.718	<u>0.786</u>
LPIPS↑		N/A	N/A	N/A	0.082	0.106

with much better inpainting realism and inpainting diversity.

4.4. Ablation Study

We study the effectiveness of the proposed BAT by conducting ablation studies over Paris StreetView [31]. In the ablation study, we remove the two key components from BAT respectively, which result in two models: 1) w/o bidirectional context, where we will get the same objective with the autoregressive model that predicts the missing tokens by conditioning on previous tokens with unidirectional attention; 2) w/o autoregressive model, where the model is equivalent to MLM that independently reconstruct the miss-

Table 3. Ablation study of the proposed BAT over Paris StreetView [31] validation set (100) with irregular masks [25] and mask ratios of 40%-60%.

Models	FID↓	ℓ_1 (%) ↓	PSNR↑	SSIM↑	LPIPS↑
w/o bidirectional	102.80	12.45	17.44	0.424	0.0551
w/o autoregressive	91.03	10.46	19.18	0.534	0.0389
Ours	87.06	10.44	19.27	0.553	0.0418

ing tokens. To measure the diversity of MLM, we employ a Gibbs sampling to iteratively sample tokens and place the predicted tokens into the original sequence instead of directly output all the predicted tokens. For a fair comparison, we apply the same irregular masks (mask ratios 40-60%) on the same low-resolution images (32×32) from the validation set of Paris StreetView [31]. After predicting the same inputs, the reconstructed structures of each model are evaluated without applying the texture generator. As shown in Table 3, using AR greatly degrades the quality of the reconstructed structures, and the high diversity measured by LPIPS is also largely attributed to the poor reconstruction quality. MLM performs reasonably well as it exploits the bidirectional context for inpainting. However, the proposed BAT clearly outperforms in both reconstruction quality and diversity that are mainly reflected by FID and LPIPS respectively. This is mainly because BAT models the output dependency to align the future predictions with previously predicted tokens and improves the consistency of the reconstructed structures. Overall, the ablation study demonstrates that the proposed BAT addresses the constraints of the two objectives AR and MLM effectively.

5. Conclusion

This paper presents BAT-Fill, a novel image inpainting framework that achieves realistic and diverse inpainting by leveraging the powerful long-dependency model-

ing of transformers and the local texture representation of CNNs. To improve the quality and diversity of inpainting, we propose a novel bidirectional and autoregressive transformer (BAT) to model the bidirectional context and output dependency simultaneously. Extensive experiments show that BAT-Fill achieves superior image inpainting in terms of both quality and diversity. Moving forward, we will explore the feasibility of adapting our idea to other image recovery or generation tasks by replacing the non-predicted part of BAT with other conditions such as semantic label, edge, and pose.

References

- [1] Coloma Ballester, Marcelo Bertalmio, Vicent Caselles, Guillermo Sapiro, and Joan Verdera. Filling-in by joint interpolation of vector fields and gray levels. *IEEE Trans. Image Process.*, 10(8):1200–1211, 2001.
- [2] Coloma Ballester, Vicent Caselles, Joan Verdera, Marcelo Bertalmio, and Guillermo Sapiro. A variational model for filling-in gray level and color images. In *ICCV*, volume 1, pages 10–16, 2001.
- [3] Connelly Barnes, Eli Shechtman, Adam Finkelstein, and Dan B Goldman. Patchmatch: a randomized correspondence algorithm for structural image editing. *ACM Transactions on Graphics (TOG)*, 28(3):1–11, 2009.
- [4] Marcelo Bertalmio, Andrea L Bertozzi, and Guillermo Sapiro. Navier-stokes, fluid dynamics, and image and video inpainting. In *CVPR*, volume 1, pages 355–355, 2001.
- [5] Marcelo Bertalmio, Guillermo Sapiro, Vincent Caselles, and Coloma Ballester. Image inpainting. In *Proceedings of the 27th annual conference on Computer graphics and interactive techniques*, pages 417–424, 2000.
- [6] Marcelo Bertalmio, Luminita Vese, Guillermo Sapiro, and Stanley Osher. Simultaneous structure and texture image inpainting. *TIP*, 12(8):882–889, 2003.
- [7] Nicolas Carion, Francisco Massa, Gabriel Synnaeve, Nicolas Usunier, Alexander Kirillov, and Sergey Zagoruyko. End-to-end object detection with transformers. *arXiv preprint arXiv:2005.12872*, 2020.
- [8] Mark Chen, Alec Radford, Rewon Child, Jeffrey Wu, Heewoo Jun, David Luan, and Ilya Sutskever. Generative pre-training from pixels. In *International Conference on Machine Learning*, pages 1691–1703. PMLR, 2020.
- [9] Soheil Darabi, Eli Shechtman, Connelly Barnes, Dan B Goldman, and Pradeep Sen. Image melding: Combining inconsistent images using patch-based synthesis. *ACM Transactions on Graphics (TOG)*, 31(4):1–10, 2012.
- [10] Jia Deng, Wei Dong, Richard Socher, Li-Jia Li, Kai Li, and Li Fei-Fei. Imagenet: A large-scale hierarchical image database. In *CVPR*, pages 248–255. Ieee, 2009.
- [11] Jacob Devlin, Ming-Wei Chang, Kenton Lee, and Kristina Toutanova. Bert: Pre-training of deep bidirectional transformers for language understanding. *arXiv preprint arXiv:1810.04805*, 2018.
- [12] Alexey Dosovitskiy, Lucas Beyer, Alexander Kolesnikov, Dirk Weissenborn, Xiaohua Zhai, Thomas Unterthiner, Mostafa Dehghani, Matthias Minderer, Georg Heigold, Sylvain Gelly, et al. An image is worth 16x16 words: Transformers for image recognition at scale. *arXiv preprint arXiv:2010.11929*, 2020.
- [13] Ian Goodfellow, Jean Pouget-Abadie, Mehdi Mirza, Bing Xu, David Warde-Farley, Sherjil Ozair, Aaron Courville, and Yoshua Bengio. Generative adversarial nets. In *Advances in Neural Information Processing Systems*, pages 2672–2680, 2014.
- [14] James Hays and Alexei A Efros. Scene completion using millions of photographs. *ACM Transactions on Graphics (TOG)*, 26(3):4–es, 2007.
- [15] Kaiming He, Xiangyu Zhang, Shaoqing Ren, and Jian Sun. Deep residual learning for image recognition. 2016.
- [16] Martin Heusel, Hubert Ramsauer, Thomas Unterthiner, Bernhard Nessler, and Sepp Hochreiter. Gans trained by a two time-scale update rule converge to a local nash equilibrium. In *Advances in Neural Information Processing Systems*, pages 6626–6637, 2017.
- [17] Satoshi Iizuka, Edgar Simo-Serra, and Hiroshi Ishikawa. Globally and locally consistent image completion. *ACM Trans. Graph.*, 36(4):1–14, 2017.
- [18] Phillip Isola, Jun-Yan Zhu, Tinghui Zhou, and Alexei A Efros. Image-to-image translation with conditional adversarial networks. In *CVPR*, pages 1125–1134, 2017.
- [19] Justin Johnson, Alexandre Alahi, and Li Fei-Fei. Perceptual losses for real-time style transfer and super-resolution. In *European Conference on Computer Vision*, pages 694–711. Springer, 2016.
- [20] Tero Karras, Timo Aila, Samuli Laine, and Jaakko Lehtinen. Progressive growing of gans for improved quality, stability, and variation. *International Conference on Learning Representations*, 2018.
- [21] Diederik P Kingma and Jimmy Ba. Adam: A method for stochastic optimization. *arXiv preprint arXiv:1412.6980*, 2014.
- [22] Diederik P Kingma and Max Welling. Auto-encoding variational bayes. *arXiv preprint arXiv:1312.6114*, 2013.
- [23] Liang Liao, Jing Xiao, Zheng Wang, Chia-Wen Lin, and Shin’ichi Satoh. Guidance and evaluation: Semantic-aware image inpainting for mixed scenes. 2020.
- [24] Chen-Hsuan Lin, Ersin Yumer, Oliver Wang, Eli Shechtman, and Simon Lucey. St-gan: Spatial transformer generative adversarial networks for image compositing. In *Proceedings of the IEEE Conference on Computer Vision and Pattern Recognition*, pages 9455–9464, 2018.
- [25] Guilin Liu, Fitsum A Reda, Kevin J Shih, Ting-Chun Wang, Andrew Tao, and Bryan Catanzaro. Image inpainting for irregular holes using partial convolutions. In *ECCV*, pages 85–100, 2018.
- [26] Hongyu Liu, Bin Jiang, Yibing Song, Wei Huang, and Chao Yang. Rethinking image inpainting via a mutual encoder-decoder with feature equalizations. In *ECCV*, 2020.
- [27] Hongyu Liu, Bin Jiang, Yibing Song, Wei Huang, and Chao Yang. Rethinking image inpainting via a mutual encoder-decoder with feature equalizations. In *ECCV*, pages 725–741, 2020.

- [28] Ziwei Liu, Ping Luo, Xiaogang Wang, and Xiaoou Tang. Deep learning face attributes in the wild. In *International Conference on Computer Vision*, pages 3730–3738, 2015.
- [29] Ilya Loshchilov and Frank Hutter. Decoupled weight decay regularization. *arXiv preprint arXiv:1711.05101*, 2017.
- [30] Kamyar Nazeri, Eric Ng, Tony Joseph, Faisal Z Qureshi, and Mehran Ebrahimi. Edgeconnect: Generative image inpainting with adversarial edge learning. *arXiv preprint arXiv:1901.00212*, 2019.
- [31] Taesung Park, Ming-Yu Liu, Ting-Chun Wang, and Jun-Yan Zhu. Semantic image synthesis with spatially-adaptive normalization. In *CVPR*, pages 2337–2346, 2019.
- [32] Deepak Pathak, Philipp Krahenbuhl, Jeff Donahue, Trevor Darrell, and Alexei A Efros. Context encoders: Feature learning by inpainting. In *CVPR*, pages 2536–2544, 2016.
- [33] Alec Radford, Jeff Wu, Rewon Child, David Luan, Dario Amodei, and Ilya Sutskever. Language models are unsupervised multitask learners. 2019.
- [34] Yurui Ren, Xiaoming Yu, Ruonan Zhang, Thomas H Li, Shan Liu, and Ge Li. Structureflow: Image inpainting via structure-aware appearance flow. In *ICCV*, pages 181–190, 2019.
- [35] Ashish Shrivastava, Tomas Pfister, Oncel Tuzel, Joshua Susskind, Wenda Wang, and Russell Webb. Learning from simulated and unsupervised images through adversarial training. In *Proceedings of the IEEE conference on computer vision and pattern recognition*, pages 2107–2116, 2017.
- [36] Kaitao Song, Xu Tan, Tao Qin, Jianfeng Lu, and Tie-Yan Liu. MpNet: Masked and permuted pre-training for language understanding. *arXiv preprint arXiv:2004.09297*, 2020.
- [37] Aravind Srinivas, Tsung-Yi Lin, Niki Parmar, Jonathon Shlens, Pieter Abbeel, and Ashish Vaswani. Bottleneck transformers for visual recognition. *arXiv preprint arXiv:2101.11605*, 2021.
- [38] Hugo Touvron, Matthieu Cord, Matthijs Douze, Francisco Massa, Alexandre Sablayrolles, and Hervé Jégou. Training data-efficient image transformers & distillation through attention. *arXiv preprint arXiv:2012.12877*, 2020.
- [39] Ashish Vaswani, Noam Shazeer, Niki Parmar, Jakob Uszkoreit, Llion Jones, Aidan N Gomez, Łukasz Kaiser, and Illia Polosukhin. Attention is all you need. In *Advances in neural information processing systems*, pages 5998–6008, 2017.
- [40] Ziyu Wan, Bo Zhang, Dongdong Chen, Pan Zhang, Dong Chen, Jing Liao, and Fang Wen. Bringing old photos back to life. In *CVPR*, pages 2747–2757, 2020.
- [41] Zhou Wang, Alan C Bovik, Hamid R Sheikh, and Eero P Simoncelli. Image quality assessment: from error visibility to structural similarity. *IEEE Transactions on Image Processing*, 13(4):600–612, 2004.
- [42] Rongliang Wu and Shijian Lu. Leed: Label-free expression editing via disentanglement. In *European Conference on Computer Vision*, pages 781–798. Springer, 2020.
- [43] Rongliang Wu, Gongjie Zhang, Shijian Lu, and Tao Chen. Cascade ef-gan: Progressive facial expression editing with local focuses. In *Proceedings of the IEEE/CVF Conference on Computer Vision and Pattern Recognition*, pages 5021–5030, 2020.
- [44] Shunxin Xu, Dong Liu, and Zhiwei Xiong. E2I: Generative inpainting from edge to image. *IEEE Trans. Circuit Syst. Video Technol.*, 2020.
- [45] Zhaoyi Yan, Xiaoming Li, Mu Li, Wangmeng Zuo, and Shiguang Shan. Shift-Net: Image inpainting via deep feature rearrangement. In *ECCV*, pages 1–17, 2018.
- [46] Zhilin Yang, Zihang Dai, Yiming Yang, Jaime Carbonell, Ruslan Salakhutdinov, and Quoc V Le. Xlnet: Generalized autoregressive pretraining for language understanding. *arXiv preprint arXiv:1906.08237*, 2019.
- [47] Jiahui Yu, Zhe Lin, Jimei Yang, Xiaohui Shen, Xin Lu, and Thomas S Huang. Generative image inpainting with contextual attention. In *Proceedings of the IEEE conference on computer vision and pattern recognition*, pages 5505–5514, 2018.
- [48] Jiahui Yu, Zhe Lin, Jimei Yang, Xiaohui Shen, Xin Lu, and Thomas S. Huang. Generative image inpainting with contextual attention. In *CVPR*, pages 5505–5514, 2018.
- [49] Jiahui Yu, Zhe Lin, Jimei Yang, Xiaohui Shen, Xin Lu, and Thomas S Huang. Free-form image inpainting with gated convolution. In *ICCV*, pages 4471–4480, 2019.
- [50] Fangneng Zhan and Shijian Lu. Esir: End-to-end scene text recognition via iterative image rectification. In *Proceedings of the IEEE Conference on Computer Vision and Pattern Recognition*, pages 2059–2068, 2019.
- [51] Fangneng Zhan, Shijian Lu, Changgong Zhang, Feiying Ma, and Xuansong Xie. Adversarial image composition with auxiliary illumination. In *Proceedings of the Asian Conference on Computer Vision*, 2020.
- [52] Fangneng Zhan, Chuhui Xue, and Shijian Lu. Ga-dan: Geometry-aware domain adaptation network for scene text detection and recognition. In *Proceedings of the IEEE International Conference on Computer Vision*, pages 9105–9115, 2019.
- [53] Fangneng Zhan, Yingchen Yu, Rongliang Wu, Changgong Zhang, Shijian Lu, Ling Shao, Feiying Ma, and Xuansong Xie. Gmlight: Lighting estimation via geometric distribution approximation. *arXiv preprint arXiv:2102.10244*, 2021.
- [54] Fangneng Zhan and Changgong Zhang. Spatial-aware gan for unsupervised person re-identification. *Proceedings of the International Conference on Pattern Recognition*, 2020.
- [55] Fangneng Zhan, Changgong Zhang, Yingchen Yu, Yuan Chang, Shijian Lu, Feiying Ma, and Xuansong Xie. Emlight: Lighting estimation via spherical distribution approximation. *AAAI*, 2020.
- [56] Fangneng Zhan, Hongyuan Zhu, and Shijian Lu. Spatial fusion gan for image synthesis. In *Proceedings of the IEEE conference on computer vision and pattern recognition*, pages 3653–3662, 2019.
- [57] Gongjie Zhang, Kaiwen Cui, Tzu-Yi Hung, and Shijian Lu. Defect-gan: High-fidelity defect synthesis for automated defect inspection. In *Proceedings of the IEEE/CVF Winter Conference on Applications of Computer Vision*, pages 2524–2534, 2021.
- [58] Richard Zhang, Phillip Isola, Alexei A Efros, Eli Shechtman, and Oliver Wang. The unreasonable effectiveness of deep features as a perceptual metric. In *CVPR*, pages 586–595, 2018.

- [59] Lei Zhao, Qihang Mo, Sihuan Lin, Zhizhong Wang, Zhiwen Zuo, Haibo Chen, Wei Xing, and Dongming Lu. Uctgan: Diverse image inpainting based on unsupervised cross-space translation. In *CVPR*, pages 5741–5750, 2020.
- [60] Shengjia Zhao, Jiaming Song, and Stefano Ermon. Towards deeper understanding of variational autoencoding models. *arXiv preprint arXiv:1702.08658*, 2017.
- [61] Chuanxia Zheng, Tat-Jen Cham, and Jianfei Cai. Pluralistic image completion. In *CVPR*, pages 1438–1447, 2019.
- [62] Bolei Zhou, Agata Lapedriza, Aditya Khosla, Aude Oliva, and Antonio Torralba. Places: A 10 million image database for scene recognition. *IEEE Transactions on Pattern Analysis and Machine Intelligence*, 2017.
- [63] Xizhou Zhu, Weijie Su, Lewei Lu, Bin Li, Xiaogang Wang, and Jifeng Dai. Deformable detr: Deformable transformers for end-to-end object detection. *arXiv preprint arXiv:2010.04159*, 2020.